ECLÉTICA QUÍMICA

Eclet. Quim. 49 | e-1497, 2024

Original Article

https://doi.org/10.26850/1678-4618.eq.v49.2024.e1497

Electrochemical sensing of uric acid using bismuth-silver bimetallic nanoparticles modified sensor

Charlton Van der **Horst**[1], Eric de Souza **Gil**[2], Vernon **Somerset**[1+]

Abstract

We showcase in this investigation a GCE/Bi–Ag electrochemical nanosensor for uric acid (UA) detection in commercial fruit juice samples. These GCE/Bi–Ag nanosensor electrochemical performances were studied using cyclic voltammetry (CV) and differential pulse voltammetry (DPV) modes showing excellent electrochemical properties toward UA detection in contrast with the clean GCE. Using the fabricated nanosensor, we exploited DPV measurements to detect UA at a meager limit of detection (0.6 µmol/L, S/N = 3) and linearity between 5.0 and 80 µmol/L UA. Furthermore, the GCE/Bi–Ag nanosensor illustrates good repeatability and reproducibility with 3.80% and RSDs of 3.22%, respectively. The GCE/Bi–Ag nanosensor was effectively exploited to determine UA in actual fruit juice samples showing excellent recoveries, indicating that it can be a promising alternative sensor for food analytical applications.

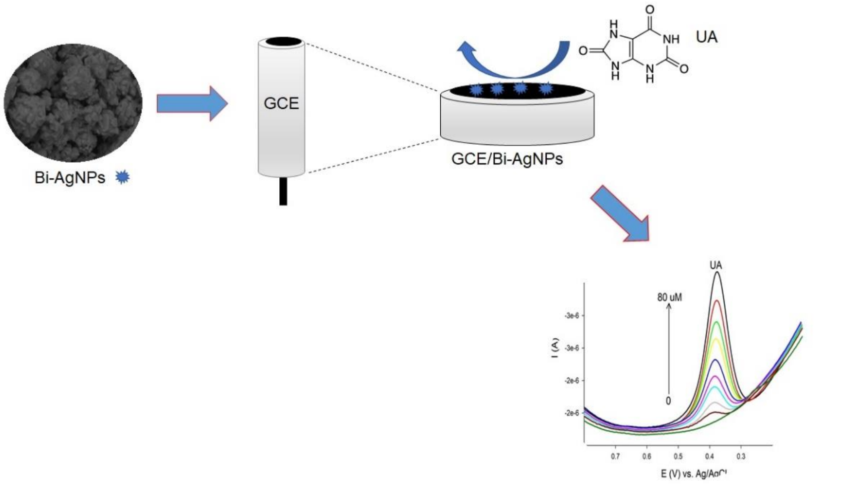

Article History

Received June 04, 2023
Accepted August 23, 2024
Published December 24, 2024

Keywords

1. GCE/Bi–AgNPs;
2. electrochemical sensor;
3. uric acid;
4. fruit juice samples.

Section Editors

Paulo Clairmont Feitosa Lima Gomes
Patricia Hatsue Suegama

Highlights

- Novel GCE/Bi–Ag nanosensor constructed for the individual detection of uric acid.
- Sensor successfully applied for electroanalysis of fruit juices.
- Nanomaterials of Bi–AgNPs have highly dispersed active sites with high surface area.
- The nanosensor obtained a detection limit of 0.6 µmol/L (S/N = 3).
- GCE/Bi–Ag nanosensor illustrates good repeatability and reproducibility.

[1]Cape Peninsula University of Technology, Faculty of Applied Sciences, Cape Town, South Africa. [2]Federal University of Goiás, Faculty of Pharmacy, Goiás, Brazil.
+Corresponding author: Vernon Somerset, **Phone:** +2721959 6116, **Email address:** vsomerset@gmail.com

1. Introduction

Uric acid (UA) or (2,6,8–trihydroxypurine) is in the human body the vital end product for the metabolism of purine and is present in blood serum and urine (Erden and Kilic, 2013; Lakshmi *et al*., 2011). The correct levels of UA in blood samples are between 0.13 to 0.46 mM and in urine between 2.49 to 4.46 mM (Huang *et al*., 2004; Raj and Ohsaka, 2001). An excess of UA in blood serum causes hypertension, gout, renal disease, and cardiovascular disease (Choi *et al*., 2005; Kanbay *et al*., 2016; Papavasileiou *et al*., 2016; Riches *et al*., 2009; Wan *et al*., 2015), whereas low levels can cause Parkinson's disease, optic disease, and Alzheimer's disease (Lakshmi *et al.*, 2011; Misra *et al.*, 2013). So, the rapid determination of uric acid (UA) with high accuracy and sensitivity using low–cost sensors in serum, urine, fruit juices, and other food products with abnormal levels of UA. It will alert concerned persons to the abnormal levels of UA and take immediate action (therapy). Medical check-ups always involve laboratory setup, bulky instrumentation, trained technicians, pre–treatment, and time do not meet this requirement.

Many analytical methods detect UA in different samples, such as chromatography (Li *et al*., 2015; Luo *et al*., 2013) and spectroscopy (Boroumand *et al.*, 2017). However, those methods require bulky instrumentation, harmful solvent, sample pre–treatment, skilled technicians, time, and cost. To overcome these drawbacks of conventional analytical methods, biosensors and electrochemical sensors have received much attention due to the advantages of high selectivity, sensitivity, and rapid response (Raj and Ohsaka, 2001). Many reports have applied various types of modified electrodes in to analyse UA samples. These various types of modified electrodes include graphene nanocomposites (Bai *et al.*, 2017; Yue *et al.*, 2015; Zhang *et al.*, 2016), modified carbon paste electrodes (Beitollahi and Sheikhshoaie, 2011; Ganesh *et al.*, 2015), multi–walled carbon nanotubes (Wayu *et al.*, 2016), quantum dots (Abbas *et al.*, 2019), polymers (Sadikoglu *et al.*, 2012), and gold nanoparticles (Ali *et al.*, 2017).

Bai *et al*. (2017) described the fabrication of a biosensor for UA detection in urine samples that includes cationic poly(diallyldimethylammonium chloride) functionalized reduced graphene oxide and polyoxometalates clusters combined with anionic Au nanoparticles. This biosensor has provided acceptable analytical features such as excellent linearity with a low detection limit. Mahmoudian *et al*. (2019) synthesized α–Fe_2O_3/polyaniline nanotube (PAnNTs) composite to construct an electrochemical nanosensor for the determination of UA in urine samples. This sensor also showed good linearity with a low detection limit. The anti–interference of the nanosensor was good by adding interfering acids such as citric acid and ascorbic acid (AA). Recently, Fukuda *et al*. (2020) have exploited a thin film biosensor that consists of carboxymethylcellulose/ uricase dispersed gold/carbon nanotube for UA detection in blood and urine samples. The constructed biosensor exhibited a low limit of detection, wide linear range, and excellent sensitivity. This report is the first individual determination of UA with other biomolecules as interferences in commercial fruit juice samples by the electrochemical measurement with GCE/Bi–Ag nanosensor.

In literature, a research group synthesized novel bismuth–silver bimetallic nanoparticles and successfully applied them in the construction of an electrochemical nanosensor and a biosensor for the detection of platinum group metals (PGMs) (Van der Horst, 2015; Van der Horst *et al.*, 2015a; 2015b; 2016a; 2017a; 2018), AA (Van der Horst *et al.*, 2016b; Van der Horst and Somerset, 2022), and hydrogen peroxide (Van der Horst *et al.*, 2017b), respectively. Recently, they also used the GCE/Bi–AgNPs nanosensor in the individual and simultaneous detection of caffeine, AA, and paracetamol in pharmaceutical formulae (Van der Horst *et al.*, 2020). These studies make the GCE/Bi–AgNPs nanosensor attractive for the individual determination of UA in commercial fruit juice samples. To date, there's no investigation reported for detecting UA in commercial fruit juice samples by the electrochemical method using Bi–AgNPs drop coated onto a glassy carbon electrode. Only AA detection in commercial fruit juice samples was reported in the literature (Brainina *et al.*, 2020; Das and Sharma, 2020).

This investigation showcases that the GCE/Bi–AgNPs nanosensor exhibited good electrocatalytic activity towards UA detection in model solutions. This GCE/Bi–AgNPs nanosensor obtained a low detection limit, excellent selectivity, wide linearity range, and high sensitivity for the detection of UA. Further, this fabricated nanosensor was utilized for UA determination with satisfactory results using commercial fruit juice samples.

2. Experimental

2.1. Materials

This investigation used analytical–grade chemicals, and we didn't purify them further. Bismuth–silver nanoparticles were prepared by adding ($Bi(NO_3)_3$) and $AgNO_3$ to HNO_3 solution. Citric acid was added to reduce the two salts to Bi–AgNPs. We prepared phosphate buffer (PB) solutions by adding NaH_2PO_4 to Na_2HPO_4, and we adjusted the pH with NaOH and H_3PO_4. UA's stock solutions were prepared by weakly dissolving UA in a freshly PB solution. Throughout this investigation, the diluting of stock solutions in freshly PB (pH = 5.0) to prepare diluted standard solutions.

2.2. Instrumentation

We performed voltammetric measurements with an Epsilon electrochemical analyzer (BASi Instruments, USA). The instrument was equipped with a conventional system of three electrodes, including a GCE/Bi–AgNPs fabricated by drop coating the Bi–AgNPs on a 1.6 mm diameter BASi disc GCE, a platinum wire that acts as the auxiliary electrode, and an Ag/AgCl/$KCl_{sat.}$ reference electrode, respectively. All experiments were performed at conditioned room temperature and in an electrochemical cell (20 mL).

2.3. Working electrode preparation

The bimetallic nanoparticles of Bi–Ag were synthesized based on the experimental procedure of our previous work (Van der Horst *et al.*, 2015a). We fabricated the GCE/Bi–AgNPs nanosensor by polishing a bare GCE in a water surrey consisting of alumina (Al_2O_3) (1.0, 0.3, and 0.05 μm) using a polishing pad. We used deionized water to rinse the clean GCE and ethanol with double distilled water for sonication. The bare GCE was further cleaned using deoxygenated aqueous H_2SO_4 (0.5 mol/L) in an electrochemical cell by applying cyclic voltammetry (CV) for 11 cycles at 100 mV/s scan rates to obtain a stable CV profile (Silwana *et al.*, 2016). Ultrasonic vibrations were used to form a suspension by dispersed bimetallic bismuth–silver nanoparticles (Bi–AgNPs) in deionized water. A small amount of Bi–AgNPs was dropped onto a clean GCE, resulting in an even Bi–AgNPs film by drying it at ambient temperature. The dried modified GCE/Bi–AgNPs sensor was slightly rinsed with deionized water, and submerged in PB (pH = 5.0), and its reproducibility was increased by scanning it for 13 cycles (Van der Horst *et al.*, 2016b).

2.4. Preparation of commercial samples

Two commercial fruit juice samples (apple and orange) were obtained at a local supermarket and the preparation was done by filtering 100 mL of the fruit juice samples in a 250 mL Erlenmeyer flask. The filtered fruit juice samples were diluted by taking 1 mL of filtered fruit juice samples in 9 mL 0.1 mol/L PB solution (pH = 5.0) in a 20 mL electrochemical cell. The diluted fruit juice samples were used for UA analysis using DPVs as the analysis mode (Benjamin *et al.*, 2015).

2.5. Determination procedure of uric acid

Phosphate buffer solution aliquots (0.1 mol/L, pH 5.0) were transferred into an electrochemical cell. Different differential pulse voltammograms were recorded by increasing concentrations from 5 to 80 μmol/L of UA in the aliquots. The cyclic voltammograms were obtained using a scan rate of 100 mV/s from −0.4 to +1.0 V (vs. Ag/AgCl) ranges. The parameters for the DPV analysis were 4 s pulse width and 50 mV pulse amplitude (Benjamin *et al.*, 2015; Van der Horst *et al.*, 2016b).

3. Results and discussion

3.1. Electrochemical characterization of constructed sensor

The electrochemical property studies of the GCE/Bi–AgNPs nanosensor were performed by using cyclic voltammetry (CV) and scan rates studies with $[Fe(CN)_6]^{3-/4-}$ solution as the electrochemistry probe. A transmission electron microscope was employed to determine the particle size of the Bi–AgNPs with diameters between 10 and 25 nanometers in **Fig. 1a**. The particle size distribution indicates that most nanoparticles were 10 and 15 nanometers (Van der Horst *et al.*, 2015a). **Figure 1b** illustrates that the modification with Bi–AgNPs increases the peak currents of the clean GCE. These phenomena may result from a large surface area and thus increase the electronic conductivity. These results illustrate that Bi–AgNPs were deposited onto the clean GCE surface by drop coating (Fukuda *et al.*, 2020; Mahmoudian *et al.*, 2019). Curve (a) (in **Fig. 1b**) of the clean GCE demonstrates a pair of redox peaks with a 142 mV peak separation.

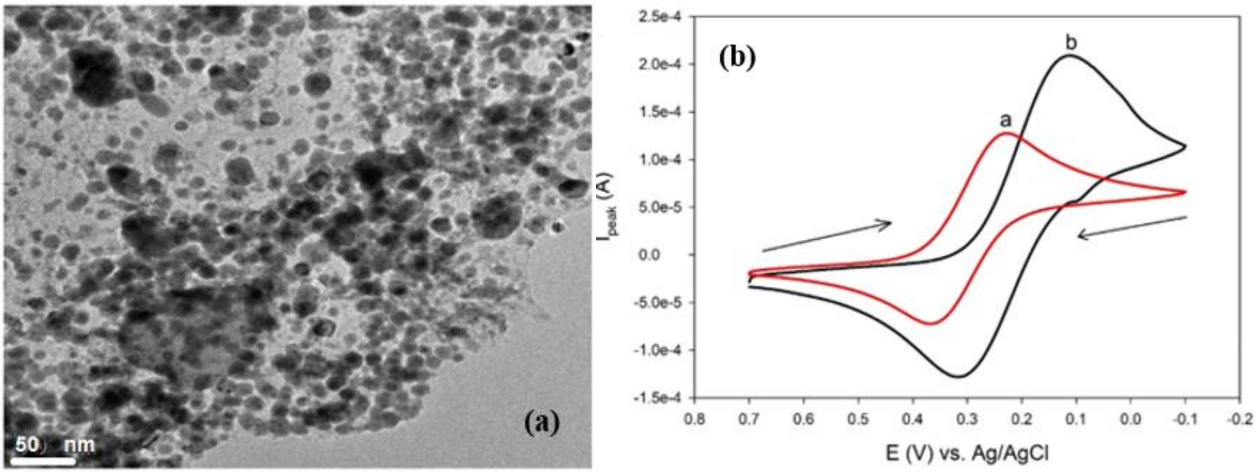

Figure 1. (a) TEM image for Bi–AgNPs; **(b)** curve a: CV curves of clean GCE; curve b: GCE/Bi–AgNPs.

Furthermore, curve (b) (in **Fig. 1b**) of the GCE/Bi–AgNPs showcases a very intense redox peak with an approximately 207 mV ΔE_p ($\Delta E_p = E_{pa} - E_{pc}$; where E_{pc} and E_{pa} stands for cathodic and anodic peak potentials) value greater than the clean GCE. These cathodic, anodic and separation peak potentials are illustrated in **Table 1**. The more excellent ΔE_p value with more significant redox peak currents at the GCE/Bi–AgNPs nanosensor showcases the superior electron transfer kinetics and sizeable active area of the Bi–AgNPs nanosensor surface.

Table 1. Illustration of the E_{pa}, E_{pc} and ΔE_p for clean GCE and GCE/Bi–AgNPs.

Electrode	E_{pa} (mV)	E_{pc} (mV)	ΔE_p
Clean GCE	368	226	142
GCE/Bi–AgNPs	318	111	207

The scan rate studies (**Fig. 2a**) were employed to study the electron transfer kinetics of the modified GCE/Bi–AgNPs electrode and the clean GCE (Makombe *et al.*, 2016). It is observed that with an increase in scan rate, the peak currents also increase along with the shifting of peak potential to greater values which is a result of the transfer of electrons between $[Fe(CN)_6]^{3-/4-}$ and the GCE/Bi–AgNPs nanosensor surface. This phenomenon results in better sensing behavior for the GCE/Bi–AgNPs nanosensor. In the calculation of the active surface area of the fabricated nanosensor, we used the Randles–Sevcik equation (**Eq. 1**),

$$I_{pa} = (2.69 \; x \; 10^5) n^{3/2} D^{1/2} C A v^{1/2} \qquad (1)$$

where n stands for the number of electrons ($n = 1$), A represents the surface area of the GCE/Bi–AgNPs nanosensor, and C is the concentration of the redox probe (1 mmol/L), D stands for the diffusion coefficient, I_{pa} stands for oxidation peak current, and v is the scan rate (V s^{-1}). We construct a profile of I_{pa} versus the square root of the scan rate ($v^{1/2}$) in **Fig. 2b**, the determined active surface area of the fabricated nanosensor was 0.150 cm^2. This active surface area of the fabricated nanosensor is much greater than the surface area of the clean GCE (0.070 cm^2). The calculated result showcase that the nanoparticles of Bi–Ag result in a vast surface area of the working electrode.

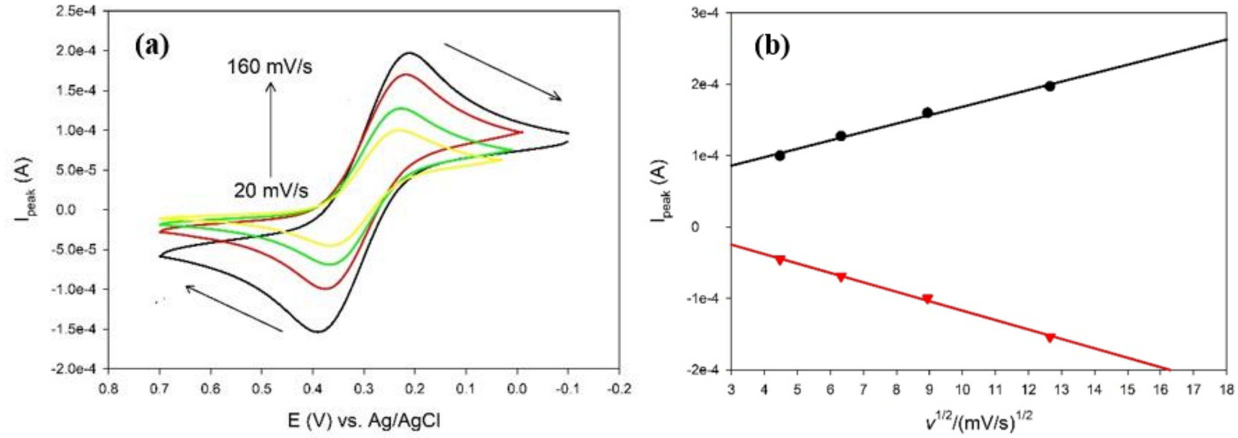

Figure 2. The study of scan rates of GCE/Bi–AgNPs in 0.1 M KCl containing 5.0 mmol/L $[Fe(CN)_6]^{3-/4-}$ in **(a)** The profile of I_{pa} vs. square root of scan rates in **(b)**.

3.2. Effect of various pHs on UA detection

The pH value is significant in detecting UA and was optimized by measuring the DPV responses of the constructed nanosensor in 80 μmol/L UA concentration. This study exploited different pH ranges of PBS to investigate the influences of the oxidation of UA peak currents. We studied the effect of pH (0.1 mol/L PB) on the DPV determination of UA in the range of pH 4.0 to pH 8.0 (N = 3). **Figure 3a** illustrates that the pH increases linearly between pH 4.0 and 5.0 and sharply declines from 5.0 to 8.0. The pH 5.0 has the highest anodic peak current responses, according to **Fig. 3a**. In this study, pH 5.0 was chosen as the optimum pH and was exploited as the supporting electrolyte in all DPV measurements. **Figure 4** illustrates the solution dependence on UA electrooxidation on the Bi–Ag/GCE nanosensor. The electrons and protons in this mechanism equally play their part in the oxidation of UA.

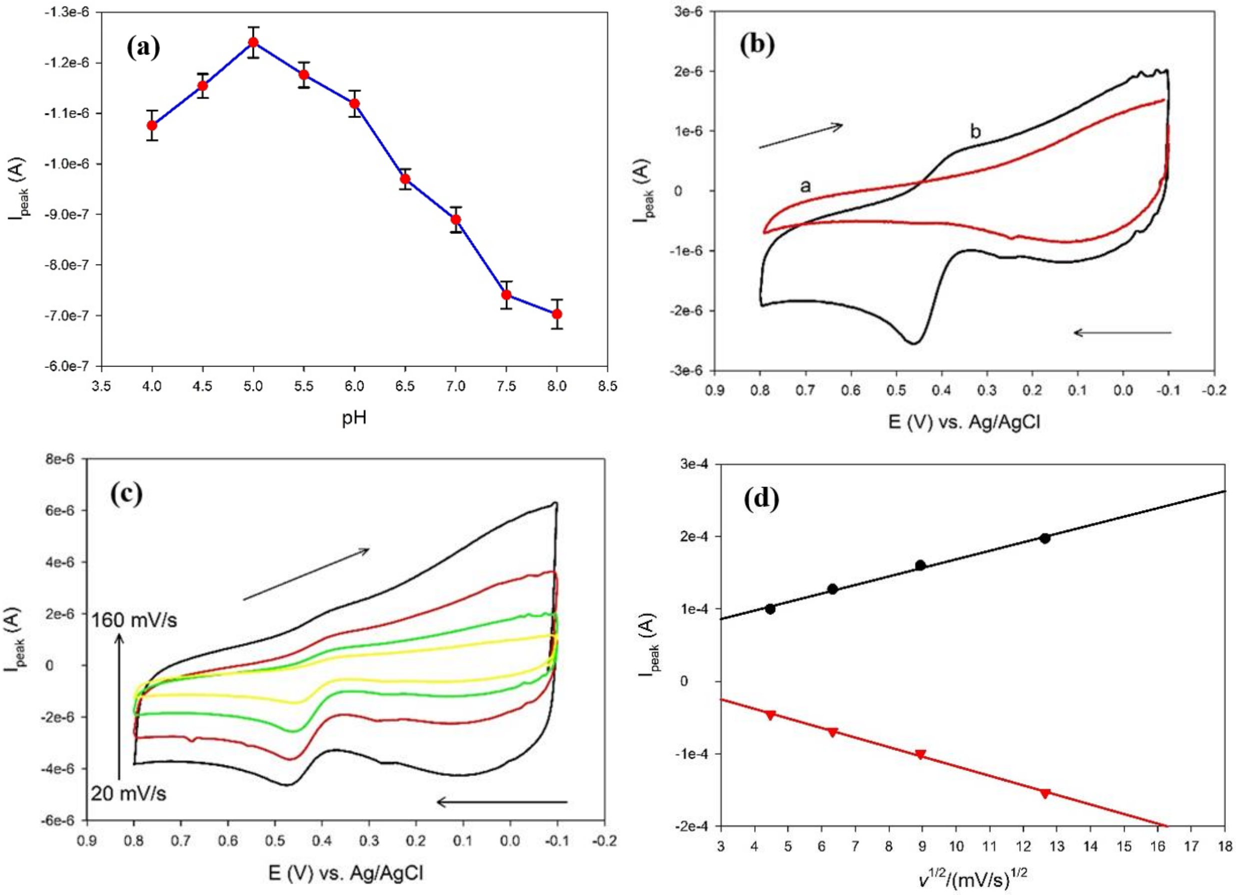

Figure 3. (a) pH optimization of 0.1 mol/L PBS; **(b)** curve a: CV curves for 80 μmol/L UA at clean GCE; curve b: constructed nanosensor; **(c)** Cyclic voltammograms for 80 μmol/L UA at GCE/Bi–AgNPs nanosensor in a 0.1 mol/L PBS (pH = 5.0) at scan rates of 20 to 160 mV s^{-1}; **(d)** Profile for peak current versus square root of scan rates.

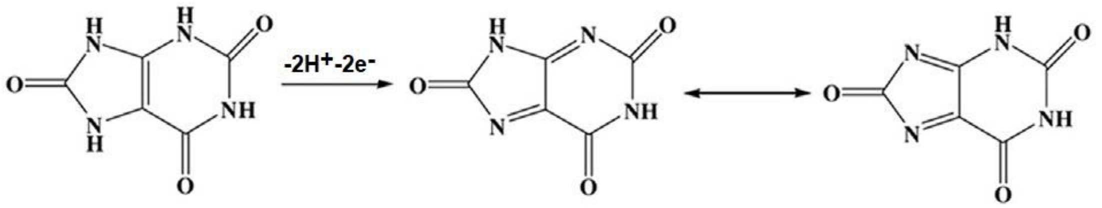

Figure 4. A Mechanism for the electrochemical oxidation of UA.

Figure 3b, we compared the CV of the constructed nanosensor with the CV of clean GCE using an 80 μmol/L UA solution. The constructed GCE/Bi–AgNPs nanosensor had a higher current response, showing that the electrochemical performance is excellent for UA sensing. The values of the anodic peak potential of UA at the GCE/Bi–AgNPs nanosensor are at about 440 mV. The chemically modified electrodes used to determine UA concentration also showed similar oxidation peak values (Liu *et al*., 2019; Makombe *et al*., 2016).

3.3 Effect of scan rates on UA detection

Cyclic voltammetry was used for scan rate studies of 80 μmol/L UA at the fabricated nanosensor in a 0.1 mol/L PBS (pH = 5.0) using increasing scan rates. As showcased in Fig. 3c, the anodic peak currents increase and shift to positive peak potentials with increasing scans of 20 to 160 mV s^{-1}. The oxidation and reduction peak currents for UA at GCE/Bi–AgNPs nanosensor generated linear profiles with linear equations are shown in Fig. 3d. We found that the oxidation peak currents versus the square root of the scan rate ($\sqrt{v}$) obey linearity. The profile equation was expressed as $I_{pa} = 2.01 \times 10^{-8}\ \nu^{1/2}$ (mV s^{-1}) – 7.0×10^{-7} ($R^2 = 0.994$) and $I_{pc} = 7.1 \times 10^{-9}\ \nu^{1/2}$ (mV s^{-1}) -3.62×10^{-8} ($R^2 = 0.998$). These equations suggest a diffusion–controlled process at the surface of the GCE/Bi–AgNPs sensor (Sangamithirai *et al*., 2018). The profile of E_{pa} and E_{pc} versus ln ν also showcase linearity with profile equations as $E_{pa} = -5.09 \times 10^{-5} \ln \nu + 1.14 \times 10^{-4}$ ($R^2 = 0.993$) and $E_{pc} = 4.63 \times 10^{-5} \ln \nu - 4.13 \times 10^{-5}$ ($R^2 = 0.996$). We used Laviron's Equations to calculate the electrochemical parameters such as n, α, and k_s, which refer to the number of electrons transferred, the electron transfer coefficient, and the standard electron transfer rate constant (Laviron, 1979).

$$E_{pa} = \frac{E^{0\prime} + 2.3RT}{(1-\alpha)nF\ log v} \quad (2)$$

$$E_{pc} = \frac{E^{0\prime} - 2.3RT}{\alpha nF\ log v} \quad (3)$$

$$log k_s = \alpha \log(1-\alpha) + (1-\alpha)\log\alpha - log(\frac{RT}{nFv}) - \frac{(1-\alpha)\alpha nF\Delta E_p}{2.3RT} \quad (4)$$

we were applying Eqs. 2 and 3, and the calculated values of n and α were reported as 2.1 and 0.87. Then, from Eq. 4, we calculated the value for k_s to be 0.61 s^{-1}.

3.4. DPV analysis of UA

Electrochemical measurements were recorded for UA in 80 μmol/L of UA model solutions at a GCE/Bi–AgNPs nanosensor, and clean GCE using DPV are demonstrated in Fig. 5a. Oxidation peak currents that are well–defined were recorded for UA in both cases. For the GCE/Bi–AgNPs electrode higher peak current value was produced and observed in the voltammogram. As followed at the clean GCE, the anodic peak potential of UA is recorded at +0.35 V (vs. Ag/AgCl), and at the fabricated nanosensor, the oxidation peak potential shifted to +0.39 V (vs. Ag/AgCl). The individual determination of UA at the fabricated nanosensor surface was investigated in a 0.1 mol/L PBS (pH 5.0) using DPV as the analytical mode. The UA oxidation peak currents in Fig. 5b increase linearly with increasing concentrations of UA under optimal experimental conditions. The constructed profile showcases that UA's linear detection range is 5 to 80 μmol/L. The profile equation is illustrated by $I_{pa\ (\mu A)} = -2.63 \times 10^{-8}\ C_{UA}$ (μmol/L) -1.59×10^{-6} with R^2 of 0.9964 and showcases the linear relationship. The detection limit measured for UA using the GCE/Bi–AgNPs nanosensor is down to 0.6 μmol/L at S/N = 3 (LOD = 3Sb/q; where Sb refers to the standard deviation of the blank and q is the slope of the linear plot). Additionally, Table 1 compares the linear range and the detection limit for the GCE/Bi–AgNPs nanosensor with other similar electrode materials. In Table 2, we concluded that the GCE/Bi–AgNPs nanosensor performance is comparable to sensors modified by other electrode materials, including linear ranges and the detection limits (LODs).

3.5 Interference studies

Possible substances in samples of natural juices that might interfere in the determination of UA at the fabricated nanosensor surface were studied by adding different ions to a 0.1 mol/L PBS (pH = 5.0). For this study, ions that might interfere, such as AA, K^+, Na^+, SO_4^{2-}, and CAF, were added to an equal amount of 40 μmol/L UA, and the sensor was immersed in the mixed solution. According to the results in Fig. 6a, AA and CAF did not show interference in the determination of UA in the presence of these interfering ions. In contrast, K^+ and Na^+ showed interference in the determination of UA in the presence of these two positive interfering ions. The anodic peak current for K^+ and Na^+ was significantly lower than that of AA and CAF. The same trend was observed for SO_4^{2-} anodic peak currents, showing that these ions interfere in UA's determination, indicating that this electrochemical sensor has reasonable specificity towards UA.

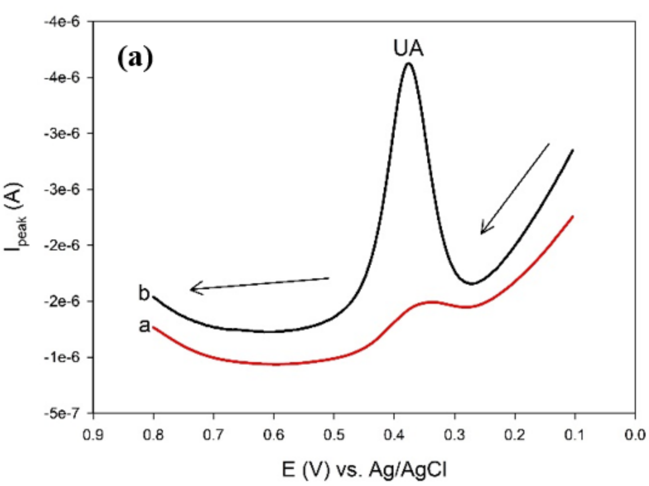

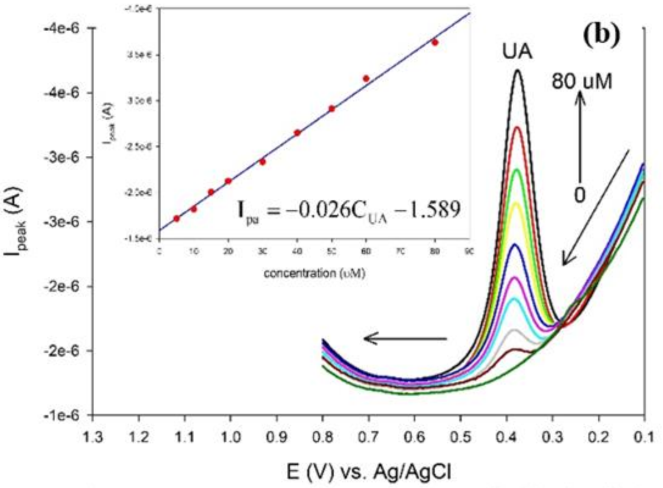

Figure 5. (a) curve a: DPV results of the clean GCE; curve b: versus the fabricated nanosensor, both in 80 µmol/L UA solution were illustrated; **(b)** the DPV results of 0.1 mol/L PBS (pH = 5.0) containing increasing concentrations of UA and (inset) the corresponding profile for UA analysis.

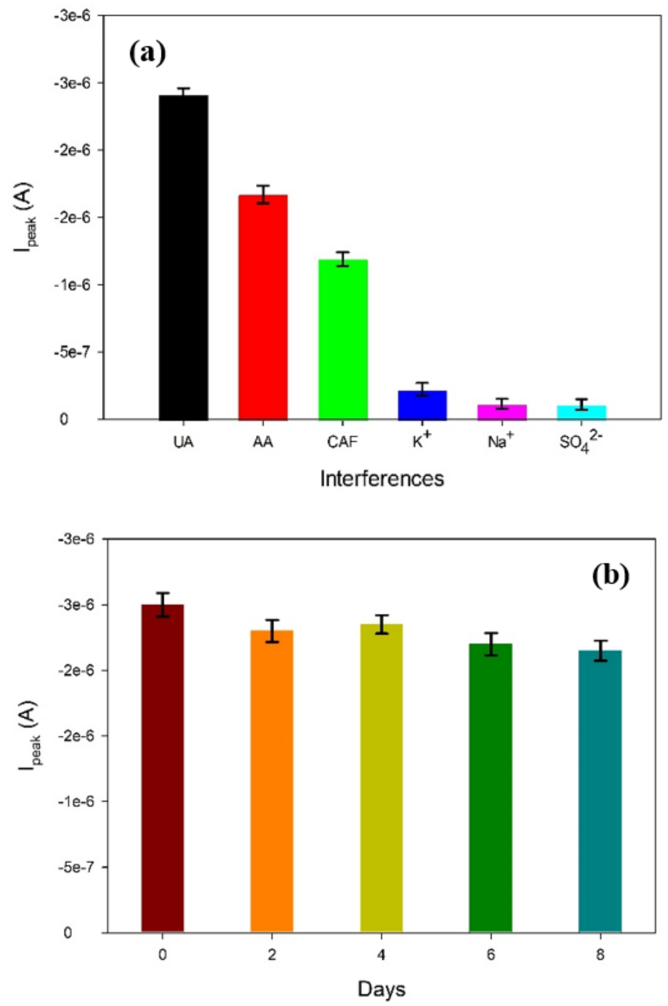

Figure 6. (a) Interference test of UA in the presence of AA, CAF, K^+, Na^+, and SO_4^{2-} that might interfere at a GCE/Bi–AgNPs nanosensor surface; **(b)** Stability tests of GCE/Bi–AgNPs nanosensor.

3.6. Effect of repeatability and stability

The repeatability, storage stability, and reproducibility of the GCE/Bi–AgNPs nanosensor were studied using the DPV measurements in 0.1 mol/L PB (pH = 5.0) containing 40 µmol/L of UA. For the storage stability study (**Fig. 6b**), the sensitivity of the fabricated sensor was measured over eight days under ambient temperature. After eight days, the nanosensor produced an anodic peak current with a slight decrease in the current response. A response current of 80% was observed after eight days. Therefore, the stability results in **Fig. 6b** of the fabricated nanosensor were good enough and resulted in continual operation.

In the case of repeatability in **Fig. 7a**, ten repetitive measurements were recorded using the same electrode with a relative standard deviation (RSD) of 3.22%. The reproducibility was also studied using six independent measurements with six different sensors constructed under similar conditions. The results obtained for the reproducibility test display a good RSD of 3.80% and are shown in **Fig. 7b**. The results (**Fig. 6b** and **7**) indicate that the fabricated nanosensor has excellent reproducibility, repeatability, and storage stability for UA detection.

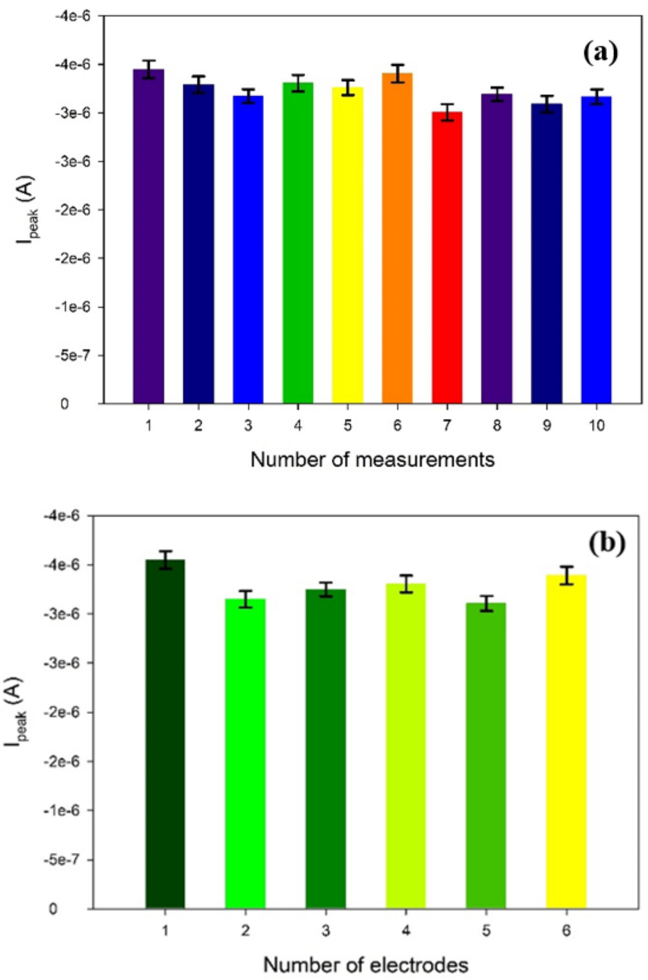

Figure 7. (a) illustrates the repeatability analysis of GCE/Bi–AgNPs nanosensor for ten repeated measurements; **(b)** the reproducibility analysis of GCE/Bi–AgNPs nanosensor for six separate electrodes.

Table 2. Illustration of the various sensors used that contain different nanomaterials in the determination of UA.

Materials	Linear ranges (µmol/L)	LOD (µmol/L)	References
PEDOT/Au NPs	1.5–150	0.08	Ali *et al.*, 2017
CNCo	2.0–110	0.83	Liu *et al.*, 2019
$PtNi@MoS_2$	0.5–600	0.1	Ma *et al.*, 2019
Ta/Ni	1.0–1400	0.1	Zhao *et al.*, 2019
a–Fe_2O_3/PAn (NTs)	0.01–5.0	0.038	Mahmoudian *et al.*, 2019
$Au1Pt_2NPs$/S–NS–GR	1–1000	0.038	Zhang *et al.*, 2018
HNP–AuAg	5–425	1.0	Hou *et al.*, 2016
ErGO/PEDOT:PSS	10–100	1.08	Wang *et al.*, 2022
2D g–C_3N_4/WO_3	0.01–900	0.0022	Rajesh *et al.*, 2022
Bi–AgNPs	5–80 µM	0.6	This study

3.7. Actual samples analysis

The developed GCE/Bi–Ag nanosensor was practically exploited for the electrochemical analysis of UA in some natural fruit juice samples by using a standard addition method. Firstly, the actual samples of fruit juices were diluted ten times with 0.1 mol/L PBS (pH 5.0). This procedure was applied before the detection of UA to decrease the matrix effect without any other treatment. After diluting, we added known quantities of standard UA to the natural fruit juice samples, and recoveries were determined. We also used Eq. 5 for the estimated recovery values of the spiked UA samples.

$$\% \text{ recoveries} = C_i \times C_o / C_x \times 100 \quad (5)$$

where C_i refers to the UA concentration experimentally obtained, C_o stands for the unspoked fruit juice samples, and C_x refers to the spiked concentration of UA in the fruit juice samples.

In Table 3, the DPV results are illustrated, showing good recoveries ranging from 98.9% to 105.1% (n = 3) and the RSDs ranging from 2.1% to 3.2% for apple juice. In the case of orange juice, the spiked UA sample recoveries ranged from 102% to 109%, with RSDs of 1.89% to 2.76%. The good recoveries for UA indicated the potential usefulness of the GCE/Bi–Ag nanosensor for the practical determination of UA in actual samples. These recovery results suggest that the electrochemical procedure has great potential for accurate, sensitive, easy, and fast detection of UA in natural fruit juice samples.

Table 3. Analysis of UA in actual fruit juice samples (n = 3) using GCE/Bi–Ag nanosensor.

Sample	Added (µmol/L)	Found (µmol/L)	Recovery (%)	RSD (%)
Apple Juice	10	10.4	104	2.1
	20	19.78	98.9	2.5
	30	31.53	105.1	3.2
Orange Juice	10	10.9	109	1.89
	20	20.7	103.5	2.76
	30	30.6	102	2.03

4. Conclusions

In summary, we have constructed an electrochemical procedure using for the first time a GCE/Bi–Ag nanosensor for the individual detection of UA in actual samples of fruit juices. The results obtained in this investigation conclude that the Bi–AgNPs have highly dispersed active sites with high surface area. These properties displayed higher peak currents for the fabricated nanosensor in contrast with the clean GCE. This phenomenon is due to enhanced electrocatalytic activity toward the oxidation of UA in model standard solutions. At the surface of the fabricated nanosensor well, distinct peaks for UA analysis were recorded with good linear regression responses of the currents for the oxidation peak. The nanosensor obtained a detection limit of 0.6 µmol/L with an $R^2 = 0.999$ for UA detection. Moreover, the GCE/Bi–Ag nanosensor brought good reproducibility, repeatability and stability, excellent anti–interference ability, and satisfied recoveries for the UA detection in actual samples.

Authors' contributions

Conceptualization: Charlton Van der Horst; Vernon Somerset; **Data curation:** Charlton Van der Horst; Vernon Somerset; **Formal Analysis:** Charlton Van der Horst; Vernon Somerset; **Funding acquisition:** Vernon Somerset; **Investigation:** Charlton Van der Horst; Vernon Somerset; **Methodology:** Charlton Van der Horst; Vernon Somerset; Eric de Souza Gil; **Project administration:** Vernon Somerset; **Resources:** Vernon Somerset; **Software:** Not applicable; **Supervision:** Vernon Somerset; **Validation:** Eric de Souza Gil; **Visualization:** Charlton Van der Horst; Vernon Somerset; Eric de Souza Gil; **Writing – original draft:** Charlton Van der Horst; Vernon Somerset; **Writing – review & editing:** Charlton Van der Horst; Vernon Somerset; Eric de Souza Gil.

Data availability statement

All data sets were generated or analyzed in the current study.

Funding

Not applicable.

Acknowledgments

The authors acknowledge the laboratory infrastructure and administrative support provided by the Cape Peninsula University of Technology (CPUT). The collaboration with the Universidade Federal de Goiás, Brazil research laboratories is greatly acknowledged.

Conflict of interest

The authors declare that there is no conflict of interest.

References

Abbas, M. W.; Soomro, R. A.; Kalwar, N. H.; Zahoor, M.; Avci, A.; Pehlivan, E.; Hallam, K. R.; Willander, M. Carbon quantum dot coated Fe_3O_4 hybrid composites for sensitive electrochemical detection of uric acid. *Microchem. J*. **2019**, *146*, 517. https://doi.org/10.1016/j.microc.2019.01.034

Ali, A.; Jamal, R.; Abdiryim, T.; Huang, X. Synthesis of monodispersed PEDOT/Au hollow nanospheres and its application for electrochemical determination of dopamine and uric acid. *J. Electroanal. Chem*. **2017**, *787*, 110. https://doi.org/10.1016/j.jelechem.2017.01.051

Bai, Z.; Zhou, C.; Xu, H.; Wang, G.; Pang, H.; Ma, H. Polyoxometalates-doped Au nanoparticles and reduced grapheneoxide: A new material for the detection of uric acid in urine. *Sens. Actuators B*. **2017**, *243*, 361. https://doi.org/10.1016/j.snb.2016.11.159

Beitollahi, H.; Sheikhshoaie, I. Electrocatalytic and simultaneous determination of isoproterenol, uric acid and folic acid at molybdenum (VI) complex-carbon nanotube paste electrode. *Electrochim. Acta*. **2011**, *56*, 10259. https://doi.org/10.1016/j.electacta.2011.09.017

Benjamin, S. R.; de Oliveira Neto, J. R.; de Macedo, I. Y. L.; Bara, M. T. F.; da Cunha, L. C.; Carvalho, L. A. F.; Gil, E. S. Electroanalysis for quality control of acerola (Malpighiaemarginata) fruits and their commercial products. *Food Anal. Methods*. **2015**, *8*, 86–92. https://doi.org/10.1007/s12161-014-9872-0

Boroumand, S.; Chamjangali, M. A.; Bagherian, G. Double injection/single detection asymmetric flow injection manifold for spectrophotometric determination of ascorbic acid and uric acid: Selection the optimal conditions by MCDM approach based on different criteria weighting methods. *Spectrochim. Acta Part A*. **2017**, *174*, 203–213. https://doi.org/10.1016/j.saa.2016.11.031

Brainina, K. Z.; Bukharinova, M. A.; Stozhko, N. Y.; Sokolkov, S. V.; Tarasov, A. V. M.; Vidrevich, M. B. Electrochemical Sensor Based on a Carbon Veil Modified by Phytosynthesized Gold Nanoparticles for Determination of Ascorbic Acid. *Sensors*. **2020**, *20*, 1800. https://doi.org/10.3390/s20061800

Choi, H. K.; Mount, D. B.; Reginato, A. M. Pathogenesis of gout. *Ann. Intern. Med*. **2005**, *143* (7), 499–516. https://doi.org/10.7326/0003-4819-143-7-200510040-00009

Das, T. R.; Sharma, P. K. Hydrothermal-assisted green synthesis of Ni/Ag@rGO nanocomposite using Punica granatum juice and electrochemical detection of ascorbic acid. *Microchem. J*. **2020**, *156*, 104850. https://doi.org/10.1016/j.microc.2020.104850

Erden, P. E.; Kilic, E. A review of enzymatic uric acid biosensors based on amperometric detection. *Talanta*. **2013**, *107*, 312–323. https://doi.org/10.1016/j.talanta.2013.01.043

Fukuda, T.; Muguruma, H.; Iwasa, H.; Tanaka, T.; Hiratsuka, A.; Shimizu, T.; Tsuji, K.; Kishimoto, T. Electrochemical determination of uric acid in urine and serum with uricase/carbon nanotube /carboxymethylcellulose electrode. *Anal. Biochem*. **2020**, *590*, 113533. https://doi.org/10.1016/j.ab.2019.113533

Ganesh, P. S.; Kumara Swamy, B. E. Simultaneous electroanalysis of norepinephrine, ascorbic acid and uric acid using poly(glutamic acid) modified carbon paste electrode. *J. Electroanal. Chem*. **2015**, *752*, 17–24. https://doi.org/10.1016/j.jelechem.2015.06.002

Hou, J.; Xu, C.; Zhao, D.; Zhou, J. Facile fabrication of hierarchical nanoporous AuAg alloy and its highly sensitive detection towards dopamine and uric acid. *Sens Actuators B*. **2016**, *225*, 241–248. https://doi.org/10.1016/j.snb.2015.11.035

Huang, S. H.; Shih, Y. C.; Wu, C. Y.; Yuan, C. J.; Yang, Y. S.; Li, Y. K.; Wu, T. K. Detection of serum uric acid using the optical polymeric enzyme biochip system. *Biosens Bioelectron*. **2004**, *19*, 1627–1633. https://doi.org/10.1016/j.bios.2003.12.026

Kanbay, M.; Jensen, T.; Solak, Y.; Le, M.; Roncal-Jimenez, C.; Rivard, C.; Lanaspa, M. A.; Nakagawa, T.; Johnson, R. J. Uric acid in metabolic syndrome: from an innocent bystander to a central player. *Eur. J. Intern. Med*. **2016**. *29*, 3–8. https://doi.org/10.1016/j.ejim.2015.11.026

Lakshmi, D.; Whitcombe, M. J.; Davis, F.; Sharma, P. S.; Prasad, B. B. Electrochemical detection of uric acid in mixed and clinical samples: a review. Electroanalysis. **2011**, *23*, 305–320. https://doi.org/10.1002/elan.201000525

Laviron, E. General expression of the linear potential sweep voltammogram in the case of diffusionless electrochemical systems. *J. Electroanal. Chem. Interfacial Electrochem*. **1979**, *101*, 19–28. https://doi.org/10.1016/S0022-0728(79)80075-3

Li, X. L.; Li, G.; Jiang, Y. Z.; Kang, D.; Jin, H.; Shi, Q.; Jin, T.; Inoue, K.; Todoroki, K.; Toyo'Oka, T. Human nails metabolite analysis: A rapid and simple method for quantification of uric acid in human fingernail by high-performance liquid chromatography with UV-detection. *J. Chromatogr. B*. **2015**, *1002*, 394–398. https://doi.org/10.1016/j.jchromb.2015.08.044

Liu, L.; Liu, L.; Wang, Y.; Ye, B-C. A novel electrochemical sensor based on bimetallic metal–organic framework-derived porous carbon for detection of uric acid. *Talanta*. **2019**, *199*, 478–484. https://doi.org/10.1016/j.talanta.2019.03.008

Luo, X.; Cai, N.; Cheng, Z. Determination of Uric Acid in Plasma by LC–MS/MS and Its Application to an Efficacy Evaluation of Recombinant Urate Oxidase. *Anal. Sci*. **2013**, *29*, 709–713. https://doi.org/10.2116/analsci.29.709

Ma, L.; Zhang, Q.; Wu, C.; Zhang, Y.; Zeng, L. PtNi bimetallic nanoparticles loaded MoS_2 nanosheets: Preparation and electrochemical sensing application for the detection of dopamine and uric acid. *Anal. Chim. Acta*. **2019**, *1055*, 17–25. https://doi.org/10.1016/j.aca.2018.12.025

Mahmoudian, M. R.; Basirun, W. J.; Sookhakian, M.; Woi, P. M.; Zalnezhad, E.; Hazarkhani, H.; Alias, Y. Synthesis and characterization of a-Fe_2O_3/polyaniline nanotube composite as electrochemical sensor for uric acid detection. *Adv. Powder Technol*. **2019**, *30*, 384–392. https://doi.org/10.1016/j.apt.2018.11.015

Makombe, M.; Van der Horst, C.; Silwana, B.; Iwuoha, E.; Somerset, V. Antimony film sensor for sensitive rare earth metal analysis in environmental samples. *J. Environ. Sci. Health Part A*. **2016**, *8*, 597–606. https://doi.org/10.1080/10934529.2016.1159857

Misra, N.; Kumar, V.; Borde, L.; Varshney, L. Localized surface plasmon resonance-optical sensors based on radiolytically synthesized silver nanoparticles for estimation of uric acid. *Sens. Actuators B*. **2013**, *178*, 371–378. https://doi.org/10.1016/j.snb.2012.12.110

Papavasileiou, M. V.; Karamanou, A. G.; Kalogeropoulos, P.; Moustakas, G.; Patsianis, S.; Pittaras, A. Uric acid blood levels and relationship with the components of metabolic syndrome in hypertensive patients. *J. Hum. Hypertens*. **2016**, *30*, 414–417. https://doi.org/10.1038/jhh.2015.53

Raj, C. R.; Ohsaka, T. Electroanalysis of ascorbate and dopamine at a gold electrode modified with a positively charged self-assembled monolayer. *J. Electroanal. Chem*. **2001**, *496 (1–2)*, 44–49. https://doi.org/10.1016/S0022-0728(00)00335-1

Rajesh, M.; Yan, W-M.; Yen, Y-K. Solvothermal synthesis of two-dimensional graphitic carbon nitride/tungsten oxide nanocomposite: a robust electrochemical scaffold for selective determination of dopamine and uric acid. *J. Appl. Electrochem*. **2022**, *52*, 1231–1248. https://doi.org/10.1007/s10800-022-01699-6

Riches, P. L.; Wright, A. F.; Ralston, S. H. Recent insights into the pathogenesis of hyperuricaemia and gout. *Hum. Mol. Genet*. **2009**, *18*, R177–R184. https://doi.org/10.1093/hmg/ddp369

Sadikoglu, M.; Taskin, G.; Demirtas, F. G.; Selvi, B.; Barut, M. Voltammetric Determination of Uric Acid on Poly(*p*-Aminobenzene Sulfonic Acid)-Modified Glassy Carbon Electrode. *Int. J. Electrochem. Sci*. **2012**, *7* (11), 11550–11557.

Sangamithirai, D.; Munusamy, S.; Narayanan, V.; Stephen, A. A voltammetric biosensor based on poly(o-methoxyaniline)-gold nanocomposite modified electrode for the simultaneous determination of dopamine and folic acid. *Mater Sci. Eng. C*. **2018**, *91*, 512–523. https://doi.org/10.1016/j.msec.2018.05.070

Silwana, B.; Van der Horst, C.; Iwuoha, E.; Somerset, V. Reduced Graphene Oxide Impregnated Antimony Nanoparticle Sensor for Electroanalysis of Platinum Group Metals. *Electroanalysis*. **2016**, *28* (7), 1597–1607. https://doi.org/10.1002/elan.201501071

Tadesse, Y.; Tadese, A.; Saini, R. C.; Pal, R. Cyclic Voltammetric Investigation of Caffeine at Anthraquinone Modified Carbon Paste Electrode. *Int J. Electrochem*. **2013**, *2013*, 1–7. https://doi.org/10.1155/2013/849327

Van der Horst, C. Development of a Bismuth-Silver Nanofilm Sensor for the Determination of Platinum Group Metals in Environmental Samples. PhD's Thesis, University of the Western Cape: Bellville, South Africa, 2015.

Van der Horst, C.; Silwana, B.; Iwuoha, E.; Somerset, V. Synthesis and characterisation of bismuth-silver bimetallic nanoparticles for electrochemical sensor applications. *Anal. Lett*. **2015a**, *48*, 1311–1332. https://doi.org/10.1080/00032719.2014.979357

Van der Horst, C.; Silwana, B.; Iwuoha, E.; Somerset, V. Bismuth-silver bimetallic nanosensor application for the voltammetric analysis of dust and soil samples. *J. Electroanal. Chem*. **2015b**, *752*, 1–11. https://doi.org/10.1016/j.jelechem.2015.06.001

Van der Horst, C.; Silwana, B.; Iwuoha, E.; Somerset, V. Application of a bismuth-silver nanosensor for the simultaneous determination of Pt-Rh and Pd-Rh complexes. *J. Nano Res*. **2016a**, *44*, 126–133. https://doi.org/10.4028/www.scientific.net/JNanoR.44.126

Van der Horst, C.; Silwana, B.; Iwuoha, E.; Gil, E.; Somerset, V. Improved detection of ascorbic acid with a bismuth-silver nanosensor. *Food Anal. Method*. **2016b**, *9*, 2560–2566. https://doi.org/10.1007/s12161-016-0444-3

Van der Horst, C. Silwana, B. Iwuoha, E. Somerset, V. Voltammetric analysis of platinum group metals using a bismuth-silver bimetallic nanoparticles sensor. In. *Recent Progress in Organometallic Chemistry*, Chapter 6; Rahman, M. M., Asiri, A. M.; Eds.; INTECH, Croatia, 2017a; pp 123. https://doi.org/10.5772/68132

Van der Horst, C.; Silwana, B.; Iwuoha, E.; Somerset, V. Electrocatalytic evaluation of a horseradish peroxidase biosensor based on a novel Bi-Ag bimetallic nanocomposite. Proc. Technol. **2017b**, *27*, 179–182. https://doi.org/10.1016/j.protcy.2017.04.077

Van der Horst, C.; Silwana, B.; Iwuoha, E.; Somerset, V. Spectroscopic and voltammetric analysis of platinum group metals in road dust and roadside soil. *Environments*. **2018**, *5* (11), 120. https://doi.org/10.3390/environments5110120

Van der Horst, C.; Silwana, B.; Gil, E.; Iwuoha, E.; Somerset, V. Simultaneous Detection of Paracetamol, Ascorbic Acid, and Caffeine Using a Bismuth-Silver Nanosensor. *Electroanalysis*. **2020**, *32*, 3098–3107. https://doi.org/10.1002/elan.202060389

Van der Horst, C.; Somerset, V. Nanoparticles Application in the Determination of Uric Acid, Ascorbic Acid, and Dopamine. *Russian J. Electrochem*. **2022**, *58*, 341–359. https://doi.org/10.1134/S102319352205010X

Wan, W.; Xu, X.; Zhao, D. B.; Pang, Y. F.; Wang, Y. X. Polymorphisms of uric transporter proteins in the pathogenesis of gout in a Chinese Han population. *Genet. Mol. Res*. **2015**, *14* (1), 2546–2550. https://doi.org/10.4238/2015.March.30.13

Wang, H.; Cao, T.; Zhou, Y.; Liu, L.; Zhang, X.; Tong, Z. A facile approach to synthesis methylene blue/reduced graphene oxide nanocomposite and simultaneous determination of dopamine and uric acid. *J. Appl. Electrochem*. **2022**, *52*, 1067–1080. https://doi.org/10.1007/s10800-022-01695-w

Wayu, M. B.; Di Pasquale, L. T.; Schwarzmann, M. A.; Gillespie, S. D.; Leopold, M. C. Electropolymerization of β-cyclodextrin onto multi-walled carbon nanotube composite films for enhanced selective detection of uric acid. *J. Electroanal. Chem*. **2016**, *783*, 192–200. https://doi.org/10.1016/j.jelechem.2016.11.021

Yue, H. Y.; Zhang, H.; Chang, J.; Gao, X.; Huang, S.; Yao, L. H.; Lin, X. Y.; Guo, E. J. Highly sensitive and selective uric acid biosensor based on a three-dimensional graphene foam/indium tin oxide glass electrode. *Anal. Biochem*. **2015**, *488*, 22–27. https://doi.org/10.1016/j.ab.2015.07.007

Zhang, K.; Chena, X.; Lia, Z.; Wang, Y.; Sun, S.; Wang, L.; Guo, T.; Zhang, D.; Xue, Z.; Zhou, Lu, X. Au-Pt bimetallic nanoparticles decorated on sulfonated nitrogen sulfur co-doped graphene for simultaneous determination of dopamine and uric acid. *Talanta*. **2018**, *178*, 315–323. https://doi.org/10.1016/j.talanta.2017.09.047

Zhang, X.; Zhang, Y-C.; Ma, L-X. One-pot facile fabrication of graphene-zinc oxide composite and its enhanced sensitivity for simultaneous electrochemical detection of ascorbic acid, dopamine and uric acid. *Sens. Actuators B*. **2016**, *227*, 488–496. https://doi.org/10.1016/j.snb.2015.12.073

Zhao, M.; Zhao, J.; Qin, L.; Jia, H.; Liu, S. Synthesis of Ta/Ni microcavity array film for highly sensitive uric acid detection. *J. Electroanal. Chem*. **2019**, *834*, 86–93. https://doi.org/10.1016/j.jelechem.2018.12.053